A preliminary version of this manuscript has been presented at the
11th International Symposium on the Future of Space Exploration
(17–19 June 2019, Torino, Italy).

Electric sail phasing maneuvers with radial thrust

Marco Bassetto*, Luisa Boni, Giovanni Mengali, Alessandro A. Quarta

Department of Civil and Industrial Engineering, University of Pisa, I-56122 Pisa, Italy

Abstract

We address the heliocentric in-orbit repositioning problem of an E-sail-based spacecraft that covers a circular parking orbit of given radius, with the assumption that the propulsive acceleration is directed along the Sun-spacecraft line. According to the recent literature, the analysis exploits the possibility of reducing the mathematical problem to the dynamics of an equivalent nonlinear oscillator with a single degree of freedom. The analytical expression of the spacecraft heliocentric trajectory, which is available in polar form when its motion is periodic, is used to obtain approximate relationships among the E-sail performance, the flight time, and the desired phasing angle. The approximate analytical model is validated through numerical simulations, whereas the last part of the paper discusses a comparison with the optimal in-orbit repositioning transfers available in the literature.

Keywords: Electric solar wind sail, radial thrust, heliocentric phasing maneuver

Nomenclature

a_c	=	characteristic acceleration, [mm/s^2]
$\{A,\, B\}$	=	dimensionless parameters; see Eqs. (14)
r	=	Sun-spacecraft distance, [au]
$r_\oplus$	=	Earth's orbital radius, (1 au)
T	=	orbital period, [days]
t	=	time, [days]
t_p	=	phasing time, [days]
x	=	auxiliary dimensionless variable; see Eq. (4)
x_C	=	dimensionless coordinate of oscillation center; see Eq. (15)
$\{\alpha_1,\, \alpha_2,\, \alpha_3\}$	=	dimensionless parameters; see Eqs. (13)
β	=	dimensionless characteristic acceleration; see Eqs. (8)
θ	=	polar angle, [deg]
$\mu_\odot$	=	Sun's gravitational parameter, [km^3/s^2]
ϕ	=	phasing angle, [deg]
ω	=	dimensionless frequency of oscillation; see Eq. (12)

Subscripts

*Corresponding author
Email addresses: marco.bassetto@ing.unipi.it (Marco Bassetto), l.boni@ing.unipi.it (Luisa Boni), g.mengali@ing.unipi.it (Giovanni Mengali), a.quarta@ing.unipi.it (Alessandro A. Quarta)

Published in Acta Astronautica, Vol. 179, February 2021, pp. 99–104. doi: https://doi.org/10.1016/j.actaastro.2020.10.025

0	=	initial

Superscripts

$\cdot$	=	time derivative
$'$	=	derivative with respect to θ
$\sim$	=	solution

1. Introduction

The Electric Solar Wind Sail (E-sail) is an innovative propellantless propulsion concept for Solar System exploration [1, 2, 3]. The E-sail generates thrust by exchanging momentum with the solar wind ions, which interact with a grid of long and electrically charged tethers. The E-sail deployment is performed by spinning the spacecraft about a longitudinal symmetry axis, and the conducting tethers are maintained at a voltage level on the order of 20 kV [4, 5] by means of an electron gun. The propulsive performance of a flat E-sail can be analytically described using the mathematical model by Huo et al. [6], according to which the thrust vector belongs to a conical region. With reference to Fig. 1, such a conical region is coaxial with the local radial direction and is characterized by an aperture angle of about 38.94 deg [6].

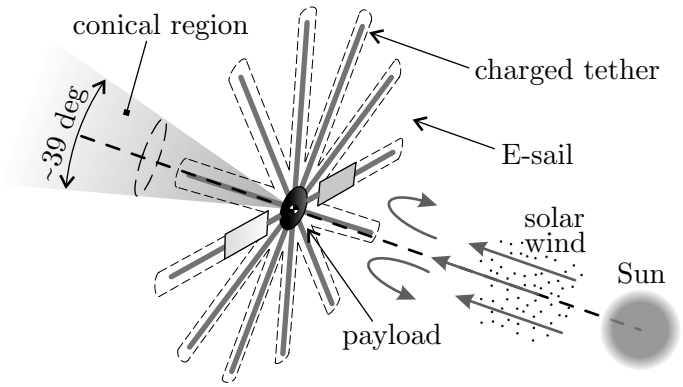

Figure 1: Conceptual scheme of the E-sail thrust vector (conical) feasible zone.

A transverse thrust may be obtained by inclining the sail nominal plane with respect to the Sun-spacecraft line, thus allowing a wide range of mission scenarios to be accomplished, such as rendez-vous with comets [7, 8] and asteroids [9, 10], the maintenance of displaced non-Keplerian orbits [11, 12], or the exploration of the Solar System's boundaries [13, 14] . However, the tether inflection due to the solar wind dynamical pressure [15, 16] makes the E-sail attitude control an involved issue and, as such, the choice of a Sun-facing configuration is the simplest way to control the E-sail attitude. Such a configuration, in which the sail nominal plane is orthogonal to the Sun-spacecraft line, is stable as the torque induced by the tether bending tends to reorient the spacecraft spin axis along the local radial direction [17, 18].

When subjected to an outward radial propulsive acceleration, an E-sail is able to perform a number of interesting mission scenarios. Some examples are offered by the maintenance of heliostationary positions [17], the formation of artificial collinear Lagrangian points, or the heliocentric in-orbit repositioning. The latter feature is useful, for example, when the mission target is to form a constellation of satellites for a 360-degree monitoring of the Sun's activity. In fact, catastrophic solar events could damage interplanetary probes or disturb the communication between the Earth and a possible future Martian ground station [19, 20]. It is therefore important to obtain an early warning of those events and to understand more deeply the phenomena related to solar activity.

The use of propellantless propulsion systems is a convenient way of performing such missions. To that end, McInnes [21] investigated the azimuthal repositioning of payloads in a heliocentric circular orbit using a solar sail. Bassetto et al. [22] analyzed the phasing maneuver of a solar sail along an elliptic heliocentric orbit, in which the phasing orbit is composed of two symmetric logarithmic spiral trajectories connected

with a single coasting arc. The same problem was also addressed in an optimal framework in Refs. [23, 24] by using a solar sail and an E-sail, respectively. The aim of this paper is to analyze the heliocentric in-orbit repositioning problem of an E-sail-based spacecraft that covers a circular orbit, assuming the propulsive acceleration vector to be aligned with the local radial direction during the whole transfer. The problem is addressed by reducing the analysis to the dynamics of an equivalent nonlinear oscillator with a single degree of freedom [25].

The paper is organized as follows. Section 2 provides the analytical polar form of the spacecraft trajectory, while the maneuver time and the phasing angle are plotted as a function of the E-sail performance parameter. Section 3 validates the presented model through a comparison of the analytical solution with some numerical simulations and optimal transfers [26] available in the recent literature. Finally, some concluding remarks are reported in the last section.

2. Mathematical model

Consider an E-sail-based spacecraft that, at the initial time $t = t_0 \triangleq 0$, covers a circular Keplerian orbit of radius $r \triangleq r_0$ around the Sun. Assume that, for $t > t_0$, the spacecraft is subjected to an outward radial propulsive acceleration of magnitude $a_c\,(r_\oplus/r)$, where a_c is the E-sail characteristic acceleration, that is, its maximum propulsive acceleration when the Sun-spacecraft distance is $r_\oplus \triangleq 1\,\text{au}$.

The spacecraft dynamics is described by the nonlinear differential equations [25]

$$\ddot{r} = -\frac{\mu_\odot}{r^2} + \frac{\mu_\odot\, r_0}{r^3} + a_c \left(\frac{r_\oplus}{r}\right) \tag{1}$$

$$\dot{\theta} = \frac{\sqrt{\mu_\odot\, r_0}}{r^2} \tag{2}$$

where $\mu_\odot \simeq 1.327 \times 10^{11}\,\text{km}^3/\text{s}^2$ is the Sun's gravitational parameter and θ is the polar angle, which is measured counterclockwise on the parking orbit plane from the Sun-spacecraft line at time t_0; see Fig. (2). In Eqs. (1)-(2), the terms $-\mu_\odot/r^2$, $\mu_\odot\, r_0/r^3$, and $a_c\, r/r_\oplus$ are the gravitational, centrifugal, and propulsive accelerations, respectively, while $\sqrt{\mu_\odot\, r_0}/r$ is the transverse component of the spacecraft velocity. Note that, the three initial conditions that complete the Cauchy problem are

$$r(t_0) = r_0 \quad , \quad \dot{r}(t_0) = 0 \quad , \quad \theta(t_0) = 0 \tag{3}$$

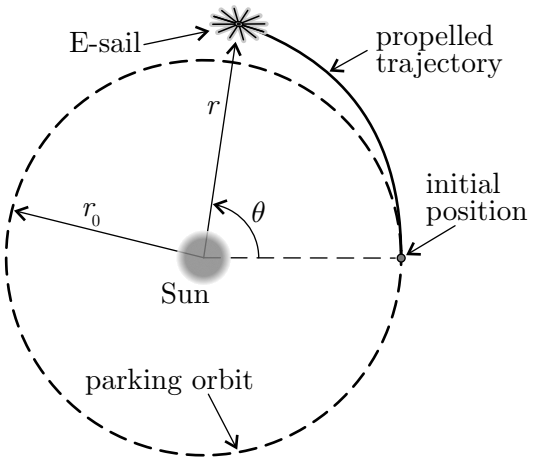

Figure 2: Polar reference frame.

The system of differential equations can be conveniently rewritten by introducing the auxiliary dimensionless variable $x \in [0,\, 1)$, defined as

$$x \triangleq 1 - \frac{r_0}{r} \tag{4}$$

and using θ as the independent variable [25]. Bearing in mind Eqs. (2)-(4), the derivatives with respect to t and θ are related to each other as

$$\frac{\mathrm{d}\xi}{\mathrm{d}t} = \frac{\sqrt{\mu_\odot\, r_0}}{r^2}\,\frac{\mathrm{d}\xi}{\mathrm{d}\theta} \equiv \sqrt{\frac{\mu_\odot}{r_0^3}}\,(1-x)^2\,\frac{\mathrm{d}\xi}{\mathrm{d}\theta} \tag{5}$$

where ξ is a generic state variable. From Eq. (5), the radial component of the velocity can be written as

$$\dot{r} = \sqrt{\frac{\mu_\odot}{r_0}}\,x' \tag{6}$$

where the prime symbol denotes a derivative with respect to θ. Accordingly, Eqs. (1)–(3) become

$$x'' = \frac{\beta}{1-x} - x \quad , \quad x'(0) = 0 \quad , \quad x(0) = 0 \tag{7}$$

where β is a sort of dimensionless characteristic acceleration, defined as

$$\beta \triangleq \frac{a_c\, r_0\, r_\oplus}{\mu_\odot} \tag{8}$$

Note that β and r_0 are mutually independent parameters, while a_c is proportional to the ratio β/r_0 through Eq. (8). In particular, when $r_0 = r_\oplus$, that is, when the circular parking orbit approximates the Earth's orbit, Eq. (8) provides $a_c = \beta\,\mu_\odot/r_\oplus^2 \simeq 5.93\,\beta\,\mathrm{mm/s^2}$.

According to the results by Nayfeh and Mook [27], Eqs. (7) describe the oscillation of a moving wire having mass m and constant length L, which is crossed by a constant electrical current i_1. The wire is restrained by a linear elastic spring with stiffness k, and is subjected to the magnetic force exerted by a fixed wire of equal length, crossed by a constant electrical current i_2; see Fig. 3, where l is the spring length at rest, $d > l$ is the (constant) distance between the left constraint and the fixed wire, and $s \in [-l,\, d-l)$ represents the displacement of the moving wire. The dynamics of the oscillating wire illustrated in Fig. 3

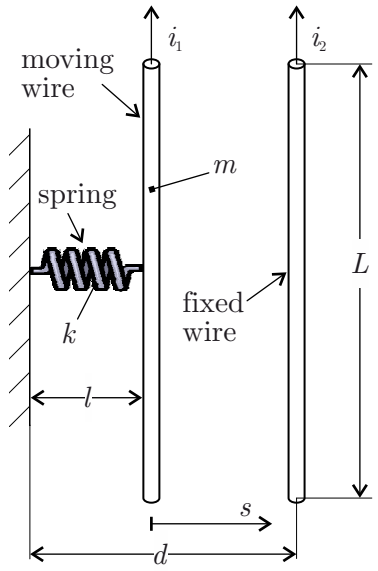

Figure 3: Current-carrying wire subjected to the magnetic force of a current-carrying conductor and to the restoring force of a spring. Adapted from Ref. [27].

is described by the second-order differential equation [27]

$$\frac{\mathrm{d}^2\delta}{\mathrm{d}\tau^2} = \frac{\lambda}{1-\delta} - \delta \quad , \quad \frac{\mathrm{d}\delta}{\mathrm{d}\tau}(0) = 0 \quad , \quad \delta(0) = 0 \tag{9}$$

where

$$\delta \triangleq \frac{s}{d-l} \quad , \quad \lambda \triangleq \frac{\mu_0\, i_1\, i_2\, L}{2\,\pi\, k\, (d-l)^2} \quad , \quad \tau \triangleq \sqrt{\frac{k}{m}}\, t \tag{10}$$

being $\mu_0 \equiv 4\,\pi \times 10^{-7}\,\mathrm{H/m}$ the vacuum permeability. Since λ is a constant parameter, Eqs. (9) are formally equivalent to Eqs. (7). The available solutions for this type of nonlinear oscillator [27, 28, 29] may therefore be effectively used to analyze the heliocentric trajectory of an interplanetary spacecraft under the outward propulsive acceleration provided by a Sun-facing E-sail. To that end, the results discussed in Ref. [25] (when specialized to the case of a circular parking orbit) are firstly used to determine an approximate expression of the spacecraft heliocentric trajectory in polar form. Starting from the approximate analytical solution, the flight time and the phasing angle are then expressed as a function of the parking orbit radius r_0 and the E-sail performance parameter β.

Paralleling the procedure described in Ref. [25], the approximate analytical solution of the differential system (7), referred to as $\widetilde{x}$, can be written as

$$\widetilde{x} = A\, \left[\cos(\omega\,\theta) - B\, \sin^2(\omega\,\theta) - 1\right] \tag{11}$$

which is a periodic function of θ with period equal to $2\,\pi/\omega$, where the approximate dimensionless frequency is given by [25]

$$\omega \triangleq \sqrt{\alpha_1}\, \left[1 + \frac{A^2\, \left(9\,\alpha_1\,\alpha_3 - 10\,\alpha_2^2\right)}{24\,\alpha_1^2}\right] \tag{12}$$

while the (dimensionless) parameters $\{\alpha_1,\, \alpha_2,\, \alpha_3,\, A,\, B\}$ are defined as

$$\alpha_1 \triangleq 1 - \frac{\beta}{(1-x_C)^2} \quad , \quad \alpha_2 \triangleq -\frac{\beta}{(1-x_C)^3} \quad , \quad \alpha_3 \triangleq -\frac{\beta}{(1-x_C)^4} \tag{13}$$

and

$$A \triangleq \frac{3\,\alpha_1 - \sqrt{9\,\alpha_1^2 + 12\,\alpha_1\,\alpha_2\,x_C}}{2\,\alpha_2} \quad , \quad B \triangleq \frac{A\,\alpha_2}{3\,\alpha_1} \tag{14}$$

with

$$x_C \triangleq \frac{1 - \sqrt{1-4\,\beta}}{2} \tag{15}$$

In particular, x_C corresponds to the (dimensionless) coordinate of the center of the equivalent oscillator [25], that is, $x_C \equiv \max(\widetilde{x})/2$. Therefore, taking Eq. (4) into account, Eq. (15) implies

$$\max(\widetilde{r}) = \frac{r_0}{\sqrt{1-4\,\beta}} \tag{16}$$

where

$$\widetilde{r} = \frac{r_0}{1 - A\, \left[\cos(\omega\,\theta) - B\, \sin^2(\omega\,\theta) - 1\right]} \tag{17}$$

is the expression of the approximate orbital radius as a function of the polar angle, that is, the polar form of the spacecraft trajectory.

2.1. Maneuver time and phasing angle

The duration t_p of the phasing maneuver corresponds to the period of the propelled trajectory and coincides with the minimum time interval that the spacecraft takes to come back to the initial circular orbit after t_0; see Fig. (4). The flight time may be obtained starting from Eq. (2) and observing that $\theta(t_p) \simeq 2\,\pi/\omega$, viz.

$$t_p \triangleq t_p(\beta, r_0) \simeq \frac{T_0}{2\,\pi} \int_0^{2\,\pi/\omega} \frac{\mathrm{d}\theta}{\left\{1 - A\, \left[\cos(\omega\,\theta) - B\, \sin^2(\omega\,\theta) - 1\right]\right\}^2} \tag{18}$$

where $T_0 \triangleq 2\,\pi\,\sqrt{r_0^3/\mu_\odot}$ is the orbital period of the circular parking orbit. Note that, in general, the approximate expression of time, referred to as $\widetilde{t}$, may be obtained as a function of θ by evaluating the integral

$$\widetilde{t}(\theta) = \frac{T_0}{2\,\pi} \int_0^{\theta} \frac{\mathrm{d}\xi}{\left\{1 - A\, \left[\cos(\omega\,\xi) - B\, \sin^2(\omega\,\xi) - 1\right]\right\}^2} \tag{19}$$

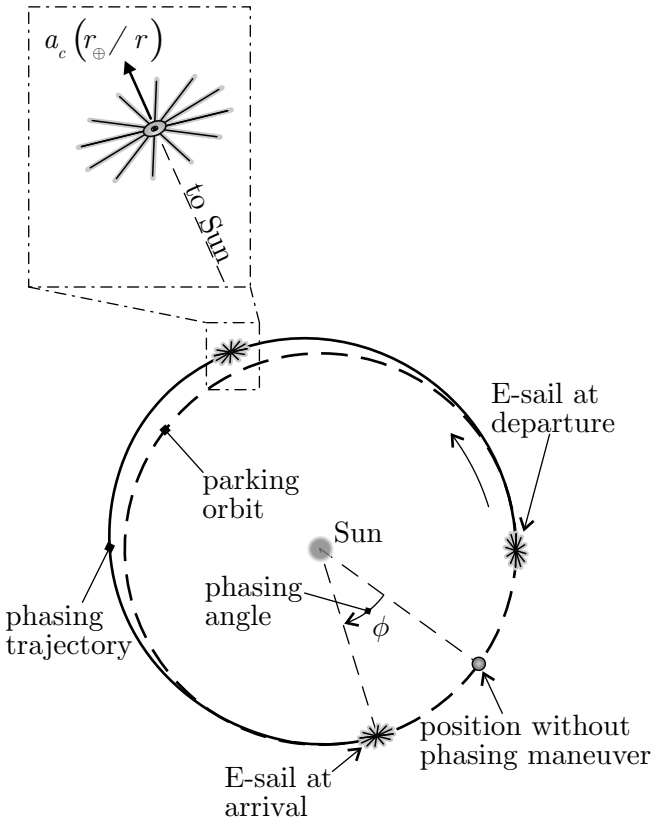

Figure 4: Conceptual scheme of a phasing maneuver with a Sun-facing E-sail.

Notably, the antiderivative of the integrating function in Eqs. (18)-(19) exists and can be determined using a symbolic computation software. However, it is not reported here as its explicit form is quite lengthy. Finally, the phasing angle ϕ is obtained as

$$\phi \triangleq \phi(\beta) \simeq \frac{2\,\pi}{\omega} - \sqrt{\frac{\mu_\odot}{r_0^3}}\,t_p \equiv \frac{2\,\pi}{\omega} - \int_0^{2\,\pi/\omega} \frac{\mathrm{d}\theta}{\left\{1 - A\,\left[\cos\left(\omega\,\theta\right) - B\,\sin^2\left(\omega\,\theta\right) - 1\right]\right\}^2} \tag{20}$$

which is independent of r_0. Figure 5 shows the plots of both t_p and ϕ as a function of $\beta \in [0,\, 0.1686]$. In particular, when $\beta = 0.1686$ and $r = r_\oplus$, then $a_c = 1\,\mathrm{mm/s^2}$, which corresponds to a medium-high performance E-sail; see Eq. (8).

Note that both the flight time and the corresponding phasing angle are obtained assuming one period of the equivalent nonlinear oscillator, while larger phasing angles may be achieved by considering two (or more) periods of the equivalent oscillator.

3. Model validation and mission application

A number of numerical simulations has been carried out in order to evaluate the effectiveness of the approximate analytical solution. To that end, Eqs. (1) and (2) have been numerically integrated with the initial conditions given by Eqs. (3) using a variable order Adams-Bashforth-Moulton PECE solver [30] with absolute and relative errors equal to 10^{-12}. The analysis has been performed for different values of r_0 and β to verify that, as expected, the soundness of the analytical solution is independent of the particular choice of r_0. Actually, the numerical simulations point out that, for any value of r_0, the difference between the maneuver time calculated with a numerical algorithm and that estimated with the analytical approximation is less than 1% when $\beta \leq 0.1003$, while the difference in the phasing angle is less than 1 deg if $\beta \leq 0.0619$.

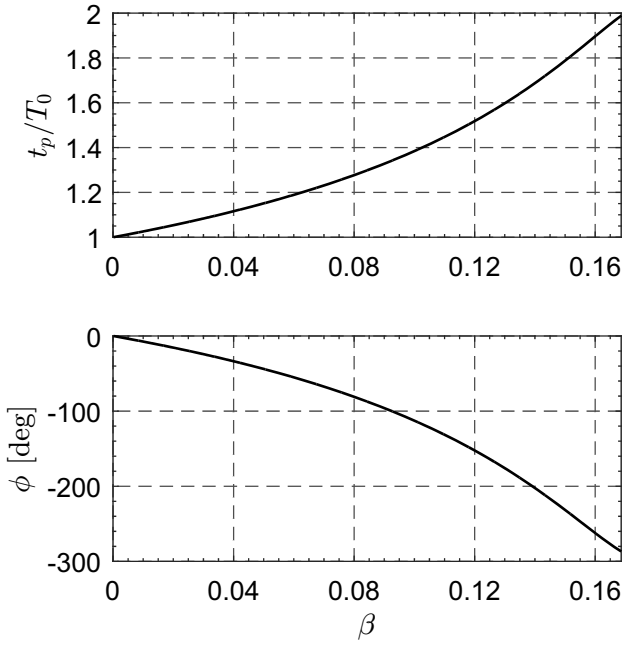

Figure 5: Maneuver time (t_p) and phasing angle (ϕ) as a function of $\beta \in [0, 0.1686]$.

Recall that, if $r_0 = r_\oplus$ and $\beta = 0.1003$ (or $\beta = 0.0619$), the value of the characteristic acceleration is $a_c = 0.594\,\mathrm{mm/s^2}$ (or $a_c = 0.367\,\mathrm{mm/s^2}$). Therefore, the accuracy of the approximate solution tends to decrease as the characteristic acceleration increases. Figure 6 shows $\{t_p, \phi\}$ as a function of $\beta \leq 0.0619$. Recall that, for a given β, the corresponding E-sail characteristic acceleration is inversely proportional to r_0; see Eq. (8).

Consider, for example, an E-sail-based spacecraft that covers a heliocentric circular orbit of radius $r_0 = r_\oplus$ and assume that $\beta = 0.0619$ (i.e., $a_c = 0.367\,\mathrm{mm/s^2}$). In this case, Tab. 1 reports the flight time and the phasing angle obtained with the approximate analytical approach and via numerical simulations, by assuming a single period of the equivalent nonlinear oscillator. The error in the phasing angle is equal to 0.998 deg, while the error in the maneuver time is about 1 day (corresponding to a relative error of about 0.23%).

	analytical	numerical
t_p [years]	1.1970	1.1998
ϕ [deg]	−57.374	−58.372

Table 1: Comparison between (approximate) analytical and numerical results, when $r_0 = r_\oplus$ and $a_c = 0.367\,\mathrm{mm/s^2}$.

3.1. Comparison with optimal results

The effectiveness of a phasing maneuver performed by an E-sail that generates an outward radial propulsive acceleration may be evaluated by a comparison with the literature results. To this regard, Refs. [24, 26] investigated heliocentric phasing maneuvers performed by an E-sail-based spacecraft within an optimal framework, that is, by looking for the minimum flight time required for the spacecraft to change its azimuthal position along a circular parking orbit. In both Refs. [24, 26], the minimum-time trajectory was obtained as a function of the E-sail characteristic acceleration and phasing angle using the nonlinear equations of motion. However, Ref. [24] used a rough E-sail thrust model [31] in which the propulsive acceleration magnitude is independent of the sail attitude and the maximum thrust angle (that is, the maximum angle

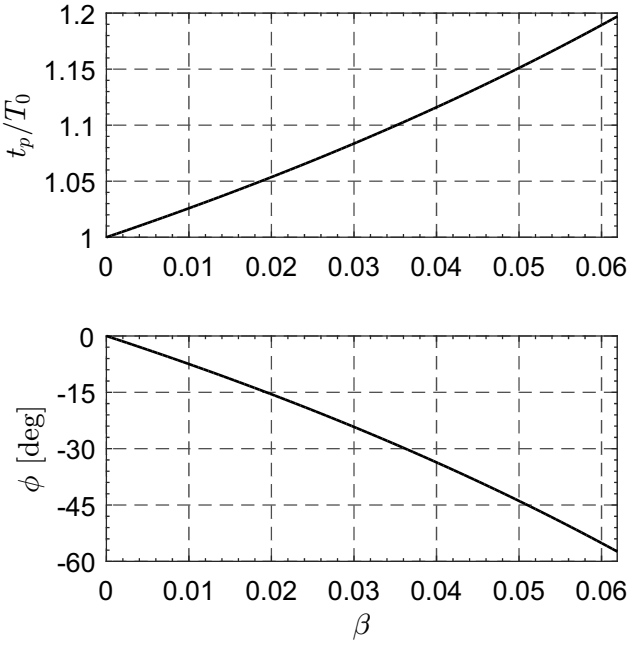

Figure 6: Maneuver time (t_p) and phasing angle (ϕ) as a function of $\beta \in [0, 0.0619]$.

between the local radial direction and the thrust vector) is equal to 30 deg. More recently, Ref. [26] adopted the refined thrust model by Huo et al. [6] in which the thrust magnitude changes with respect to the sail attitude and the maximum thrust angle is about 19.47 deg; see Fig. 1. Accordingly, a comparison with the results presented in Ref. [26] is more meaningful. In particular, the comparison with the numerical results of Ref. [26] will be made by considering the same initial conditions in terms of spacecraft position and velocity components.

To that end, assume $r_0 = r_\oplus$ and consider, for example, an E-sail-based spacecraft with $a_c = 0.1\,\mathrm{mm/s^2}$ (i.e., $\beta \simeq 0.0169$). In this case, the phasing angle is $\phi = -13\,\mathrm{deg}$, and the corresponding flight time is about 381.6 days; see Fig. 6. Using the same value of β, the optimal approach discussed in Ref. [26] provides a minimum flight time of about 359.5 days to phase back the spacecraft by $-13\,\mathrm{deg}$. In other terms, the flight time obtained with the proposed approach is about 6% greater than the optimal (i.e., minimum) one, which is achievable when the E-sail has not attitude constraints. In any case, a small increase of the required maneuver time may be acceptable for the advantage of a much simpler steering law [32].

4. Conclusions

We have investigated the heliocentric repositioning problem of an E-sail-based spacecraft on a circular parking orbit. The main assumption is that the E-sail provides an outward radial propulsive acceleration during the whole transfer. The spacecraft equations of motion have been reduced to the dynamics of an equivalent nonlinear oscillator with a single degree of freedom by means of a suitable change of variable. The approximate polar form of the spacecraft trajectory has allowed us to find a relationship between the E-sail performance, the maneuver time, and the phasing angle.

The resulting analytical solution is accurate enough when sufficiently small values of the dimensionless characteristic acceleration are considered. The maneuver times are slightly longer than the optimal ones available in the literature for this type of scenario, but with the advantage that they are obtained with a much simpler steering law.

References

[1] P. Janhunen, Electric sail for spacecraft propulsion, Journal of Propulsion and Power 20 (4) (2004) 763–764, doi: 10.2514/1.8580.

[2] P. Janhunen, A. Sandroos, Simulation study of solar wind push on a charged wire: basis of solar wind electric sail propulsion, Annales Geophysicae 25 (3) (2007) 755–767, doi: 10.5194/angeo-25-755-2007.

[3] P. Janhunen, P. K. Toivanen, J. Polkko, et al., Electric solar wind sail: Towards test missions, Review of Scientific Instruments 81 (11) (2010) 111301 (1–11), doi: 10.1063/1.3514548.

[4] P. Janhunen, Status report of the electric sail in 2009, Acta Astronautica 68 (5-6) (2011) 567–570, doi: 10.1016/j.actaastro.2010.02.007.

[5] K. Yamaguchi, K. Miyata, Orbital maneuvering of electric solar wind sail based on an advanced solar wind force model, Acta Astronautica 166 (2020) 417–430, doi: 10.1016/j.actaastro.2019.10.001.

[6] M. Huo, G. Mengali, A. A. Quarta, Electric sail thrust model from a geometrical perspective, Journal of Guidance, Control, and Dynamics 41 (3) (2018) 735–741, doi: 10.2514/1.G003169.

[7] A. A. Quarta, G. Mengali, P. Janhunen, Electric sail option for cometary rendezvous, Acta Astronautica 127 (2016) 684–692, doi: 10.1016/j.actaastro.2016.06.020.

[8] M. Bassetto, A. A. Quarta, G. Mengali, Locally-optimal electric sail transfer, Proceedings of the Institution of Mechanical Engineers, Part G: Journal of Aerospace Engineering, 233 (1) (2019) 166–179, doi: 10.1177/0954410017728975.

[9] A. A. Quarta, G. Mengali, Electric sail missions to potentially hazardous asteroids, Acta Astronautica 66 (9-10) (2010) 1506–1519, doi: 10.1016/j.actaastro.2009.11.021.

[10] G. Mengali, A. A. Quarta, Optimal nodal flyby with near-Earth asteroids using electric sail, Acta Astronautica 104 (2) (2014) 450–457, doi: 10.1016/j.actaastro.2014.02.012.

[11] L. Niccolai, A. A. Quarta, G. Mengali, Electric sail-based displaced orbits with refined thrust model, Proceedings of the Institution of Mechanical Engineers, Part G: Journal of Aerospace Engineering 232 (3) (2018) 423–432, doi: 10.1177/0954410016679195.

[12] L. Niccolai, A. Anderlini, G. Mengali, A. A. Quarta, Electric sail displaced orbit control with solar wind uncertainties, Acta Astronautica 162 (2019) 563–573, doi: 10.1016/j.actaastro.2019.06.037.

[13] G. Mengali, A. A. Quarta, P. Janhunen, Electric sail performance analysis, Journal of Spacecraft and Rockets 45 (1) (2008) 122–129, doi: 10.2514/1.31769.

[14] A. A. Quarta, G. Mengali, Electric sail mission analysis for outer solar system exploration, Journal of Guidance, Control, and Dynamics 33 (3) (2010) 740–755, doi: 10.2514/1.47006.

[15] P. K. Toivanen, P. Janhunen, Thrust vectoring of an electric solar wind sail with a realistic sail shape, Acta Astronautica 131 (2017) 145–151, doi: 10.1016/j.actaastro.2016.11.027.

[16] L. Boni, M. Bassetto, G. Mengali, A. A. Quarta, Electric sail static structural analysis with finite element approach, Acta Astronautica 175 (2020) 510–516, doi: 10.1016/j.actaastro.2020.06.009.

[17] M. Bassetto, G. Mengali, A. A. Quarta, Stability and control of spinning electric solar wind sail in heliostationary orbit, Journal of Guidance, Control, and Dynamics 42 (2) (2018) 425–431, doi: 10.2514/1.G003788.

[18] M. Bassetto, G. Mengali, A. A. Quarta, Attitude dynamics of an electric sail model with a realistic shape, Acta Astronautica 159 (2019) 250–257, doi: 10.1016/j.actaastro.2019.03.064.

[19] M. Macdonald, R. J. McKay, M. Vasile, F. De Frescheville, J. D. Biggs, C. R. McInnes, Low-thrust-enabled highly-non-Keplerian orbits in support of future Mars exploration, Journal of Guidance, Control, and Dynamics 34 (5) (2011) 1396–1411, doi: 10.2514/1.52602.

[20] P. Janhunen, S. Merikallio, M. Paton, EMMI - Electric solar wind sail facilitated manned Mars initiative, Acta Astronautica 133 (2015) 22–28, doi: 10.1016/j.actaastro.2015.03.029.

[21] C. R. McInnes, Azimuthal repositioning of payloads in heliocentric orbit using solar sails, Journal of Guidance, Control, and Dynamics 26 (4) (2003) 662–664, doi: 10.2514/2.5098.

[22] M. Bassetto, L. Niccolai, A. A. Quarta, G. Mengali, Logarithmic spiral trajectories generated by solar sails, Celestial Mechanics and Dynamical Astronomy 130 (2) (2018) 18 (1–24), doi: 10.1007/s10569-017-9812-6.

[23] A. A. Quarta, G. Mengali, Optimal solar sail phasing trajectories for circular orbit, Journal of Guidance, Control, and Dynamics 36 (6) (2013) 1821–1824, doi: 10.2514/1.59372.

[24] G. Mengali, A. A. Quarta, G. Aliasi, Heliocentric phasing performance of electric sail spacecraft, Acta Astronautica 127 (2016) 474–481, doi: 10.1016/j.actaastro.2016.06.033.

[25] A. A. Quarta, G. Mengali, Analysis of electric sail heliocentric motion under radial thrust, Journal of Guidance, Control, and Dynamics 39 (6) (2016) 1431–1435, doi: 10.2514/1.G001632.

[26] L. Niccolai, A. Caruso, A. A. Quarta, G. Mengali, Electric sail phasing maneuvers for constellation deployment, In press. Acta Astronautica (2019), doi: 10.1016/j.actaastro.2019.12.003.

[27] A. H. Nayfeh, D. T. Mook, Nonlinear Oscillations, Wiley Classics Library, New York, 1995, Ch. 2, pp. 67–71.

[28] W. P. Sun, C. W. Lim, B. S. Wu, C. Wang, Analytical approximate solutions to oscillation of a current-carrying wire in a magnetic field, Nonlinear Analysis: Real World Applications 10 (3) (2009) 1882–1890, doi: 10.1016/j.nonrwa.2008.02.028.

[29] S. S. Ganji, A. Barari, A. Fereidoon, S. Karimpour, On the behaviour of current-carrying wire-conductors and bucking of a column, Mechanika 19 (3) (2013) 306–315, doi: 10.5755/j01.mech.19.3.4659.

[30] L. F. Shampine, M. W. Reichelt, The MATLAB ODE suite, SIAM Journal on Scientific Computing 18 (1) (1997) 1–22, doi: 10.1137/S1064827594276424.

[31] P. Janhunen, The electric solar wind sail status report, in: EPSC Abstracts, Vol. 5, European Planetary Science Congress, 2010, paper EPSC 2010-297.

[32] G. Li, Z. H. Zhu, C. Du, S. A. Meguid, Characteristics of coupled orbital-attitude dynamics of flexible electric solar wind sail, Acta Astronautica 159 (2019) 593–608, doi: 10.1016/j.actaastro.2019.02.009.